Short Communication:

Silicon Carbide/Polysilazane Composite: Effect of Temperature on the Densification, Phase, and Microstructure Evolution

Fiqhi Fauzi[1], Alfian Noviyanto[1,2*], Pipit Fitriani[1], Amirudin Wibowo[3], Toto Sudiro[4], Didik Aryanto[4], and Nurul Taufiqu Rochman[5]

[1]*Nano Center Indonesia, Jl. PUSPIPTEK, South Tangerang, Banten 15314, Indonesia*

[2]*Department of Mechanical Engineering, Mercu Buana University, Jl. Meruya Selatan, Kebun Jeruk, Jakarta 11650, Indonesia*

[3]*Research Center, Mercu Buana University, Jl. Meruya Selatan, Kebun Jeruk, Jakarta 11650, Indonesia*

[4]*Research Center for Physics, National Research and Innovation Agency, PUSPIPTEK, South Tangerang, Banten 15314, Indonesia*

[5]*Research Center for Metallurgy and Materials, National Research and Innovation Agency, PUSPIPTEK, South Tangerang, Banten 15314, Indonesia*

Corresponding author:

email: a.noviyanto@nano.or.id

Received: September 14, 2021
Accepted: October 29, 2021

DOI: 10.22146/ijc.69118

Abstract: *This paper reports a route to suppress the grain growth in silicon carbide (SiC) during its sintering by combining it with polysilazane (PSZ). SiC was mixed with PSZ in a 1:1 weight ratio and sintered at 1600, 1700, and 1800 °C in a hot-pressing furnace. A satisfactory density was obtained at sintering temperatures > 1600 °C. The grain sizes of the SiC/PSZ composites sintered at 1700 and 1800 °C were 112 and 125 nm, respectively. The grain shape of the SiC/PSZ composite sintered at 1700 °C was circular and mainly similar to the initial shape of the SiC powder. Grain shape accommodation was observed at a sintering temperature of 1800 °C. It is suggested that different sample shapes were affected by different liquid phase formations. Silicon oxynitride (Si_2N_2O) was formed and played an important role in densification and microstructure generation.*

Keywords: *silicon carbide; polysilazane; sintering; microstructure*

■ INTRODUCTION

Silicon carbide (SiC) is being studied as a non-oxide ceramic engineering material. SiC has high thermal conductivity, low thermal expansion, resistance to oxidation and corrosion, and high hardness. Owing to its strong covalent bonding, SiC has excellent properties. In particular, given that the hardness of SiC is lower than those of diamond and cubic boron nitride, SiC is widely used as an abrasive material. However, the sintering of SiC is complex, requiring a high temperature and pressure to obtain a dense microstructure. For instance, the sintering of SiC through solid-state requires temperatures ≥ 1900 °C [1-13], whereas liquid-phase sintering requires a temperature range of 1750–1900 °C [14-20]. Although a dense SiC body can be achieved under such sintering conditions, the microstructure of SiC undergoes coarsening. According to the Hall–Petch relationship, a fine microstructure is proportional to high hardness; therefore, there is a need to minimize grain coarsening during its high-temperature sintering.

Typically, there are two approaches for minimizing the grain coarsening of the microstructure of SiC produced by high-temperature sintering. First, high pressure can be applied. For instance, Xie et al. reported that nanograin SiC could be successfully obtained at 1300 °C by applying a pressure of 4.5 GPa [21]. The second approach is a two-step sintering process; Lee et al. reported that SiC with a grain size of 43 nm could be obtained by two-step sintering [22]. However, the first approach requires ultra-high pressure, and the second one is time-consuming. The other method is the use of sintering additives that hinder the grain growth of SiC

during sintering. For example, Noviyanto et al. reported that a scandium-based additive could help minimize the grain growth in SiC [23]. Other reports show that polysilazane (PSZ, $[-SiR_1R_2NH-]_n$) can suppress the grain growth of alumina dan hafnia [24-25]. Noviyanto et al. examined a SiC/PSZ composite [26]. However, the effect of temperature on the SiC/PSZ composite was not elucidated.

In this study, SiC/PSZ composites were sintered using a hot-pressing furnace in the temperature range of 1600–1800 °C for 1 h under an applied pressure of 20 MPa in a nitrogen atmosphere. In addition, the effects of polysilazane on the densification, phase, and microstructure were thoroughly investigated. Finally, a mechanism to suppress grain growth with polysilazane was proposed in this study.

■ EXPERIMENTAL SECTION

Materials

β-SiC powder (D_m = 52 nm, 4620KE, 97.5% purity, NanoAmor Inc., USA), polysilazane (KiON Ceraset Polysilazane 20, USA), Al_2O_3 (99.9% purity, Baikowski, Japan) and Y_2O_3 (99.99% purity, Across Organic, USA) were used in this study.

Instrumentation

X-ray diffraction (XRD: X'Pert-PRO MPD, PANalytical, The Netherlands) and scanning electron microscope (SEM: S-4800, Hitachi, Japan) were used in this study.

Procedure

Prior to mixing with β-SiC powder, polysilazane was dissolved in acetone. Subsequently, β-SiC powder was added, and the solution was homogenized using an ultrasonicator for 45 min. The weight ratio of polysilazane to β-SiC powder was 1:1. Next, the homogenized slurry was dried and cross-linked on a hot plate at 200 °C for 90 min to obtain a powder containing β-SiC and polysilazane. After grinding and sieving, the powder was pyrolyzed in a tube furnace at 1300 °C for 2 h in a nitrogen atmosphere to transform the polysilazane into amorphous powder. This temperature was chosen because the crystallization of amorphous polysilazane starts at 1400 °C [27-28].

Furthermore, the powder containing β-SiC and amorphous polysilazane was ground and sieved, followed by mixing with sintering additives (Al_2O_3 and Y_2O_3, with a weight ratio of 60:40). The amount of sintering additives was 5 wt.% with respect to the total mass of the powder. Ball milling was used to mix the powder and sintering additives for 24 h and was made from SiC to prevent contamination. The sintering was performed in a hot-pressing furnace at various temperatures for 1 h under an applied pressure of 20 MPa in a nitrogen atmosphere. The samples were named SiCPSZ1600, SiCPSZ1700, and SiCPSZ1800, corresponding to the mixture containing β-SiC powder and polysilazane sintered at 1600, 1700, and 1800 °C, respectively. For comparison, the sintered SiC without adding polysilazane and sintered amorphous polysilazane were also prepared at 1750 and 1800 °C, respectively, named SiC and PSZ.

The weight of the sintered samples was measured at room temperature and when immersed in distilled water. The data were used to estimate the density of the sintered samples using the Archimedes principle. Furthermore, the sintered samples were characterized by room-temperature XRD to observe the crystalline phase formed after sintering. The qualitative and quantitative analyses of the XRD pattern were performed by XRD software analysis to determine the phases and their composition. Finally, the sintered samples were crushed, and the fractured surface was observed using SEM. The average grain size was estimated by calculating 100 grains from the SEM images and analyzed statistically.

■ RESULTS AND DISCUSSION

Fig. 1 shows the XRD patterns of the SiC/PSZ composite after sintering. The patterns of β-SiC and α-SiC can be detected at 1600 °C (Fig. 1(a)). As listed in Table 1, the major phases detected in SiCPSZ1600 were α-SiC (COD #96-900-0037) and β-SiC (COD #96-101-0966), accounting for 57.1% and 35.2%, respectively. To understand the phase transformation of β- and α-SiC in SiCPSZ1600, we need to compare with the sintering of

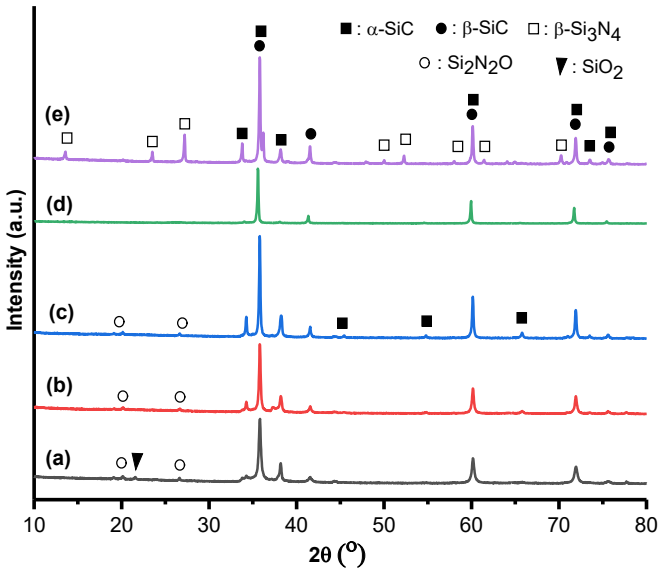

Fig 1. XRD patterns of the sintered sample (a) SiCPSZ1600, (b) SiCPSZ1700, (c) SiCPSZ1800, (d) SiC, and (e) PSZ

SiC and PSZ, as shown in Fig. 1(d) and 1(e), respectively. Sintering of the β-SiC powder resulted in a β-SiC phase; however, small peaks of α-SiC were detected, as shown in Fig. 1(d). The α-SiC phase in sintered SiC is more likely from the transformation of β- to α-SiC phase, which typically occurs in high-temperature sintering [29]. The quantity of α-SiC in the sintered SiC was 20.6% (Table 1).

In contrast, the sintering of PSZ results in a predominant α-SiC phase (55.6%) along with β-SiC and Si_3N_4 (COD #96-100-1245), as shown in Fig. 1(e). Thus, the main source of α-SiC in SiCPSZ1600 is more likely from polysilazane that tends to form α-SiC instead of β-SiC. The other phases detected in SiCPSZ1600 were Si_2N_2O (COD #96-901-2533) and SiO_2 (COD #96-100-1245). Polysilazane might form SiC, Si_3N_4, or SiO_2 depending on the temperature and atmosphere condition. This Si_2N_2O phase is the product of a reaction between Si_3N_4 and SiO_2 [30]. Subsequently, the source of SiO_2 derives from polysilazane itself or SiC that has a small thin layer of oxide on the surface. According to the Gibbs free energy, the existence of Si_3N_4 from polysilazane is more favorable at < 1500 °C compared with SiC. Fig. 1(b) shows that the presence of SiO_2 could not be detected in SiCPSZ1700. SiO_2 completely reacted with Si_3N_4 to form Si_2N_2O or decomposed at high temperatures and nitrogen atmosphere.

As listed in Table 1, the proportion of Si_2N_2O in SiCPSZ1700 increases. Furthermore, Si_2N_2O phase decreased in SiCPSZ1800. Si_2N_2O is thermally unstable and starts to decompose at a high temperature of 1850 °C [30]. A similar phenomenon has been reported for $LaTiO_2N$, which decomposed during high-temperature sintering to La_2O_3 and TiN [31]. The final composition of the phases in SiCPSZ1800 are α-SiC, β-SiC, and Si_2N_2O, with the major phase being α-SiC, as listed in Table 1. On the other hand, the sintering of PSZ led to the formation of a SiC/Si_3N_4 composite, as shown in Fig. 1(e). No trace of Si_2N_2O could be detected in the sintering of SiC and PSZ. The absence of SiO_2 phase in PSZ and Si_3N_4 phase in SiC makes the formation of Si_2N_2O unattainable.

Table 1 shows the quantitative analysis of the sintered samples' XRD, density, and relative density. The density increased with increasing temperature. However, the densification of the SiC/PSZ composite requires temperatures >1600 °C. The density of SiCPSZ1600 was 2.48 g/cm^3, corresponding to 77.2% of the relative density. Although the sintered sample was mixed with 5 wt.% of

Table 1. Quantitative analysis of the XRD patterns, density, and relative density of sintered samples

Sample	Phase composition (wt.%)					Density (g/cm^3)	Relative density (%)*
	β-SiC	α-SiC	Si_2N_2O	SiO_2	Si_3N_4		
SiCPSZ1600	35.2	57.1	7.2	0.3	-	2.48 ± 0.18	78.1
SiCPSZ1700	31.4	56.3	12.3	-	-	3.02 ± 0.01	95.5
SiCPSZ1800	27.8	69.4	2.8	-	-	3.05 ± 0.07	95.5
SiC	79.4	20.6	-	-	-	3.19 ± 0.01	99.3
PSZ	11.8	55.6	-	-	32.6	3.17 ± 0.04	98.7

*Relative density was calculated by comparing the density of samples with their theoretical density, according to the rule of mixture

additives, it seems that the temperature was too low for liquid-phase formation; therefore, the density of SiCPSZ1600 did not increase. In contrast, the density of the samples sintered at temperatures > 1600 °C significantly increased, as listed in Table 1. The density and relative density of SiCPSZ1700 were 3.02 g/cm^3 and 94.1%, respectively. No significant increase in the density of the samples sintered at 1800 °C was observed, i.e., the density of SiCPSZ1800 was 3.05 g/cm^3. Therefore, a liquid-phase formation is believed to have occurred in SiCPSZ1700 and SiCPSZ1800, causing densification.

The source of the liquid phase is generally the sintering additives. The sintering additives, i.e., Al_2O_3–Y_2O_3, form a liquid phase at 1760 °C [32]. Therefore, the densification of SiCPSZ1700 is more likely due to another liquid phase, not Al_2O_3–Y_2O_3. As reported, the formation of Si_2N_2O occurs through a liquid phase [30,33-36]; hence, the liquid phase enhances the densification in SiCPSZ1700.

Fig. 2 shows the SEM images of the sintered SiC/PSZ composites at various temperatures. Clearly, pores were observed in the composite SiCPSZ1600 (Fig. 2(a)), which showed a low sintered solid body. On the other hand, dense sintered bodies were obtained from SiCPSZ1700 and SiCPSZ1800. Remarkably, the average grain sizes of SiCPSZ1700 and SiCPSZ1800 were 112 ± 40 and 125 ± 62 nm, respectively, which increased by a factor of two from the initial particle size of the β-SiC

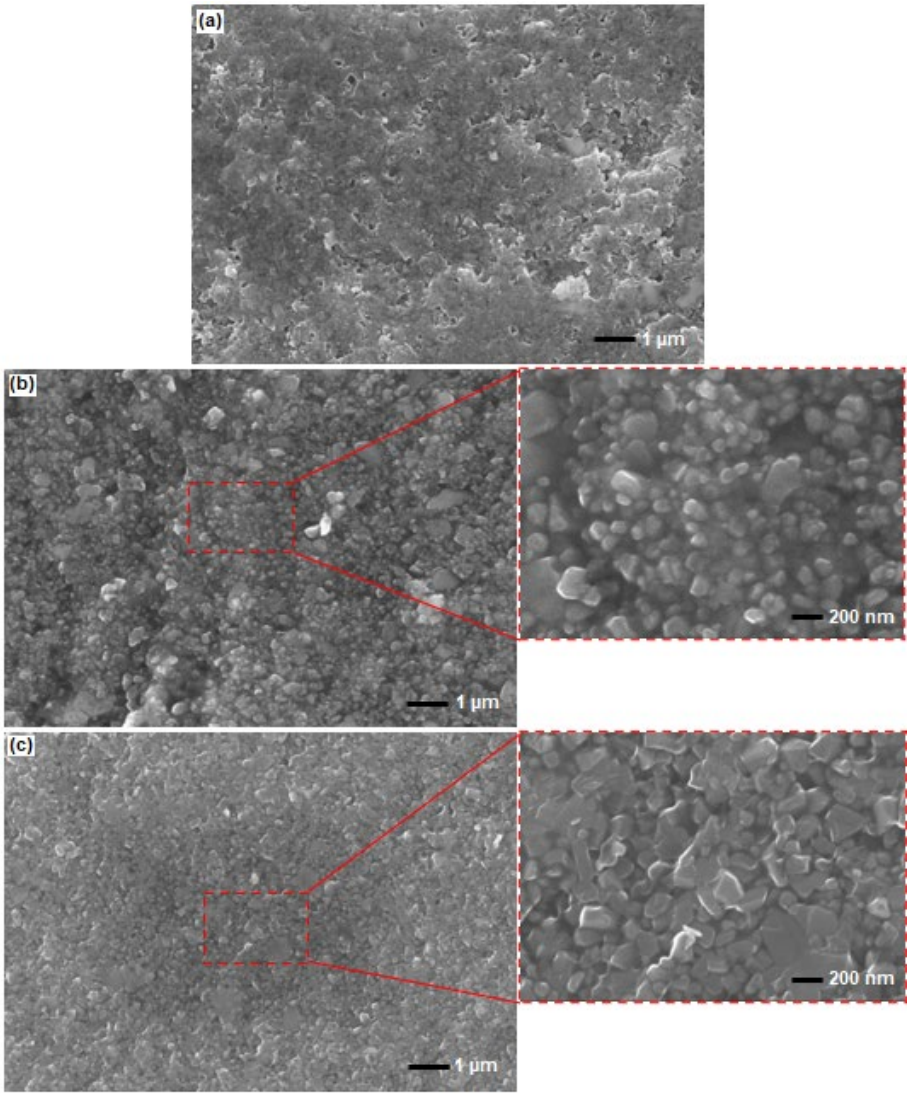

Fig 2. SEM images of SiC/PSZ composites sintered at temperatures of (a) 1600, (b) 1700, and (c) 1800 °C

powder. Although the densities of SiCPSZ1700 and SiCPSZ1800 were similar, the microstructures of the prepared samples were considerably different. The grain shape of SiCPSZ1700 (Fig. 2(b)) was close to the initial shape of SiC, i.e., round, whereas an equiaxed grain was observed in SiCPSZ1800 (Fig. 2(c)). The difference in the microstructures is more likely induced by the liquid phase that forms during sintering. As explained previously, the liquid phase of Si_2N_2O appears at a lower temperature than the liquid phase of Al_2O_3–Y_2O_3. Hence, the microstructure in SiCPSZ1700 is more likely influenced by the presence of liquid-phase Si_2N_2O. Meanwhile, equiaxed grain in SiCPSZ1800 is affected by the presence of liquid-phase Al_2O_3–Y_2O_3. A similar microstructure with SiCPSZ1800 is also observed for SiC and PSZ, as shown in Fig. 3(b) and 3(c), respectively. Therefore, it seems that the densification process of SiCPSZ1700 occurs because of the rearrangement stage without proceeding to the shape accommodation stage.

In contrast, SiCPSZ1800 reaches the shape accommodation stage, even though it seems to be at the beginning of the stage, owing to which the relative density slightly improves compared with SiCPSZ1700. Densification via the rearrangement stage is possible because of the high capillary force for a small particle size system [37]. Fig. 3(b) shows a typical SiC microstructure with the addition of Al_2O_3–Y_2O_3 sintered at 1750 °C. Grain coarsening can be observed in the sintering of SiC. A finer microstructure was obtained when sintering with PSZ (Fig. 3(c)). However, the SiC and PSZ microstructures are larger than that of SiCPSZ1800, as shown in Fig. 3(a). Since the difference in these samples is the presence of Si_2N_2O, Si_2N_2O plays an important role in inhibiting excessive grain growth, as in SiC without polysilazane. The densities of SiC and PSZ were 3.19 and 3.17 g/cm^3, respectively, higher than that of the SiC/PSZ composite. Subsequently, the liquid phase of Al_2O_3–Y_2O_3 is more effective in enhancing densification than liquid Si_2N_2O. The liquid formation is not the only factor affecting densification. Other factors, such as the low contact angle, low dihedral angle, volume fraction of liquid, the high solubility of solid in liquid, homogenous packing of the particulate solid, homogenous distribution of the liquid phase, and fairly fine particle size are also important for densification [38].

Fig. 4 shows a schematic of the densification of the SiC/PSZ composite at different temperatures. Under the initial condition, the β-SiC powder is covered by a thin layer of SiO_2 on the SiC surface. Furthermore, after mixing with dissolved polysilazane, it is assumed that an

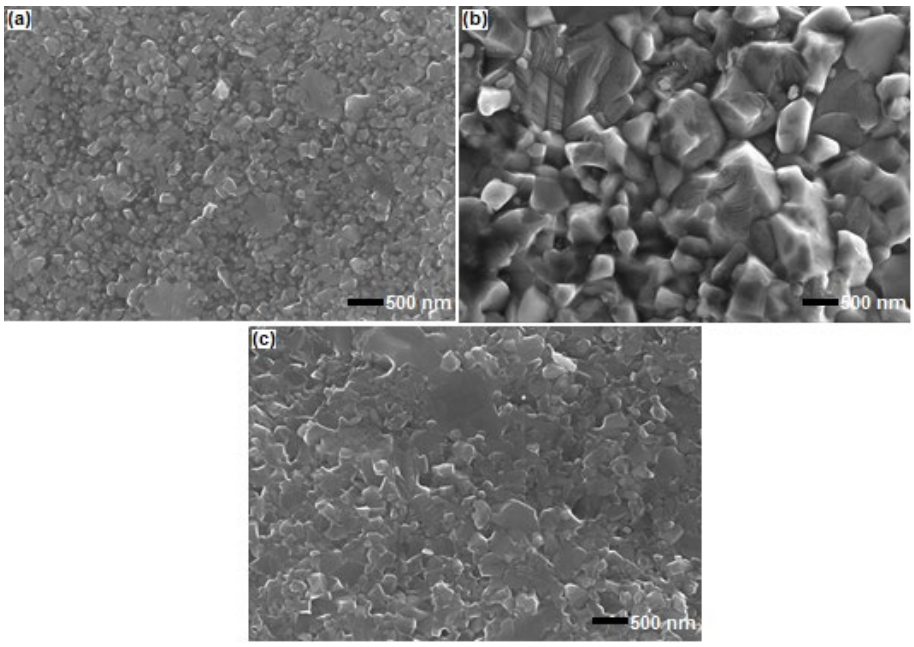

Fig 3. SEM images of sintered (a) SiCPSZ1800, (b) SiC, and (c) PSZ

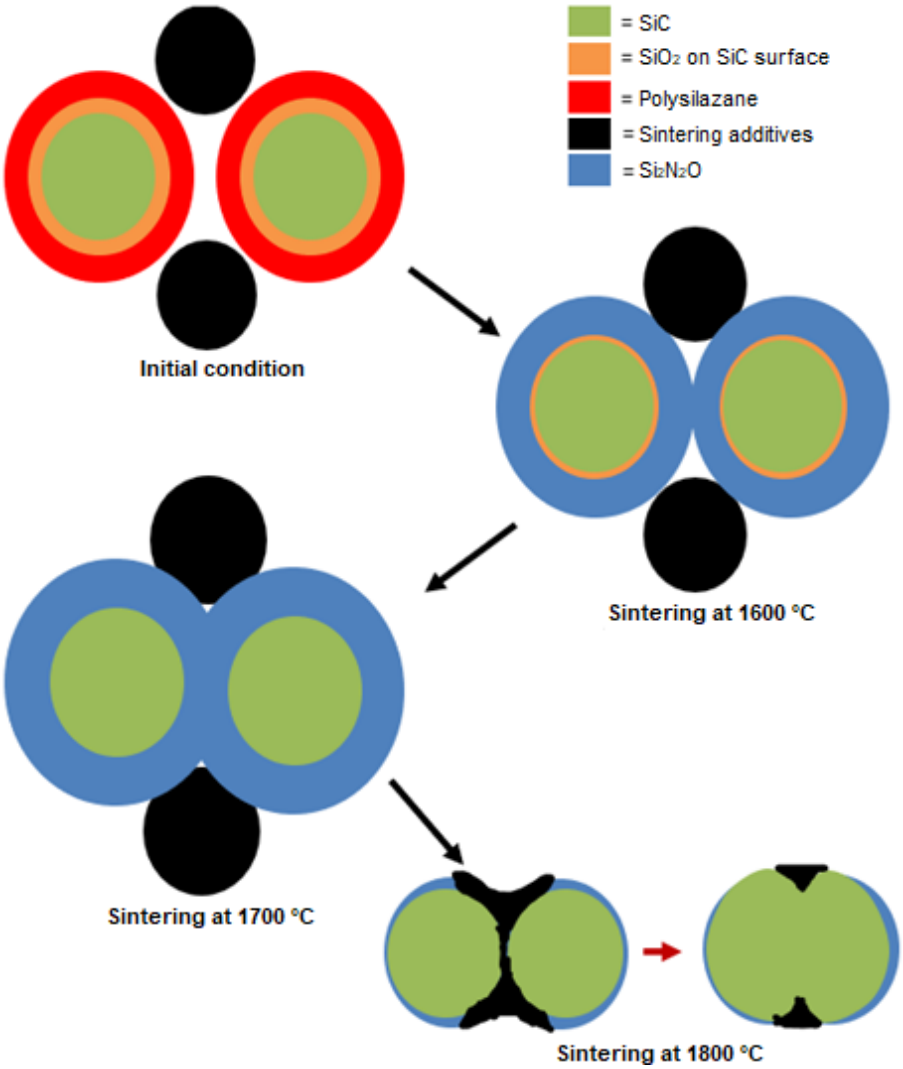

Fig 4. Schematic of the densification of SiC/PSZ composite at different temperatures

amorphous layer of polysilazane also completely covers the β-SiC powder. Si_2N_2O is detected at 1600 °C, with a small amount of SiO_2 still detected. Although the liquid phase of Si_2N_2O is already formed at this temperature, the amount of Si_2N_2O is insufficient to aid the densification, resulting in a low relative density. The relative density considerably increased to 94.1% at 1700 °C owing to the sufficient amount of Si_2N_2O. In this state, densification occurs without any change in the initial shape of SiC. The sintering additives, i.e., Al_2O_3–Y_2O_3, maintain their shape since the melting point of these additives is 1760 °C. Shape accommodation occurs at 1800 °C, and the role of sintering additives appears at this temperature.

■ CONCLUSION

SiC/PSZ composites were successfully sintered at various temperatures. A density higher than 90% could be achieved at temperatures > 1600 °C. Phase generation during sintering played a significant role in the densification process. The formation of liquid-phase Si_2N_2O was responsible for enhancing the densification of the SiC/PSZ composite at temperatures as low as 1700 °C. Moreover, densification at 1700 °C helped minimize grain growth. The grain size of the SiC/PSZ composite at 1700 °C only increased by a factor of two from the initial particle size of the SiC powder. Sintering at higher temperatures increased the density as well as the grain

growth. However, the grain size was considerably finer compared with that obtained after the sintering of SiC or PSZ. Therefore, SiC/polysilazane is suitable to obtain the dense body and fine microstructure ceramic compared to monolithic SiC sinter at 1750 °C with coarse microstructure. Indeed, the fine microstructure is essential to enhance the mechanical properties of ceramics.

■ ACKNOWLEDGMENTS

This work was financially supported by Kerjasama Dalam Negeri Scheme (KDN) [grant number 02-5/531/B-SPK/II/2021], Mercu Buana University.

■ AUTHOR CONTRIBUTIONS

FF: Writing the original draft. AN: Conceptualization, methodology, conducted the experiment, formal analysis, visualization, supervision, writing - review & editing. PF: Formal analysis. AW: Project administration. TS: Formal analysis. DA: Formal analysis and resources. NTR: Resources. All authors agreed to the final version of this manuscript.

■ REFERENCES

[1] Malik, R., and Kim, Y.W., 2021, Pressureless solid-state sintering of SiC ceramics with BN and C additives, *J. Asian Ceram. Soc.*, 9 (3), 1165–1172.

[2] Grasso, S., Saunders, T., Porwal, H., and Reece, M., 2015, Ultra-high temperature spark plasma sintering of α-SiC, *Ceram. Int.*, 41 (1), 225–230.

[3] Kultayeva, S., Kim, Y.W., and Song, I.H., 2021, Effects of dopants on electrical, thermal, and mechanical properties of porous SiC ceramics, *J. Eur. Ceram. Soc.*, 41 (7), 4006–4015.

[4] Petrus, M., Wozniak, J., Jastrzębska, A., Kostecki, M., Cygan, T., and Olszyna, A., 2018, The effect of the morphology of carbon used as a sintering aid on the sinterability of silicon carbide, *Ceram. Int.*, 44 (6), 7020–7025.

[5] Aygüzer Yaşar, Z., DeLucca, V.A., and Haber, R.A., 2021, Effect of boron carbide additive and sintering temperature - Dwelling time on silicon carbide properties, *Ceram. Int.*, 47 (5), 7177–7182.

[6] Liu, M., Yang, Y., Wei, Y., Li, Y., Zhang, H., Liu, X., and Huang, Z., 2019, Preparation of dense and high-purity SiC ceramics by pressureless solid-state-sintering, *Ceram. Int.*, 45 (16), 19771–19776.

[7] Gross, E., Dahan, D.B., and Kaplan, W.D., 2015, The role of carbon and SiO_2 in solid-state sintering of SiC, *J. Eur. Ceram. Soc.*, 35 (7), 2001–2005.

[8] Li, Y., Wu, H., Liu, X., Huang, Z., and Jiang, D., 2019, Microstructures and properties of solid-state-sintered silicon carbide membrane supports, *Ceram. Int.*, 45 (16), 19888–19894.

[9] Jana, D.C., Sundararajan, G., and Chattopadhyay, K., 2018, Effective activation energy for the solid-state sintering of silicon carbide ceramics, *Metall. Mater. Trans. A*, 49 (11), 5599–5606.

[10] Wu, H., Yan, Y., Liu, G., Liu, X., Zhu, Y., Huang, Z., Jiang, D., and Li, Y., 2015, Effects of grain grading on microstructures and mechanical behaviors of pressureless solid-state-sintered SiC, *Int. J. Appl. Ceram. Technol.*, 12 (5), 976–984.

[11] Malinge, A., Coupé, A., Le Petitcorps, Y., and Pailler, R., 2012, Pressureless sintering of beta silicon carbide nanoparticles, *J. Eur. Ceram. Soc.*, 32 (16), 4393–4400.

[12] Malinge, A., Coupé, A., Jouannigot, S., Le Petitcorps, Y., Pailler, R., and Weisbecker, P., 2012, Pressureless sintered silicon carbide tailored with aluminium nitride sintering agent, *J. Eur. Ceram. Soc.*, 32 (16), 4419–4426.

[13] Zapata-Solvas, E., Bonilla, S., Wilshaw, P.R., and Todd, R.I., 2013, Preliminary investigation of flash sintering of SiC, *J. Eur. Ceram. Soc.*, 33 (13-14), 2811–2816.

[14] Ribeiro, S., Gênova, L.A., Ribeiro, G.C., Oliveira, M.R., and Bressiani, A.H.A., 2016, effect of heating rate on the shrinkage and microstructure of liquid phase sintered SiC ceramics, *Ceram. Int.*, 42 (15), 17398–17404.

[15] Noviyanto, A., and Yoon, D.H., 2013, Rare-earth oxide additives for the sintering of silicon carbide, *Diamond Relat. Mater.*, 38, 124–130.

[16] Noviyanto, A., and Yoon, D.H., 2013, Metal oxide additives for the sintering of silicon carbide: Reactivity and densification, *Curr. Appl Phys.*, 13 (1), 287–292.

[17] Liang, H., Yao, X., Zhang, J., Liu, X., and Huang, Z., 2014, Low temperature pressureless sintering of α-SiC with Al_2O_3 and CeO_2 as additives, *J. Eur. Ceram. Soc.*, 34 (3), 831–835.

[18] Liang, H., Yao, X., Zhang, J., Liu, X., and Huang, Z., 2014, The effect of rare earth oxides on the pressureless liquid phase sintering of α-SiC, *J. Eur. Ceram. Soc.*, 34 (12), 2865–2874.

[19] Candelario, V.M., Moreno, R., Shen, Z., Guiberteau, F., and Ortiz, A.L., 2017, Liquid-phase assisted spark-plasma sintering of SiC nanoceramics and their nanocomposites with carbon nanotubes, *J. Eur. Ceram. Soc.*, 37 (5), 1929–1936.

[20] Yang, Z., Li, B., Zhang, P., Chu, M., Bai, B., Tang, H., Zhong, Y., Liu, X., Gao, R., Liu, T., and Huang, H., 2020, Microstructure and thermal physical properties of SiC matrix microencapsulated composites at temperature up to 1900 °C, *Ceram. Int.*, 46 (4), 5159–5167.

[21] Xie, M.L., Luo, D.L., Xian, X. Bin, Leng, B.Y., Chang'an, C., and Lu, W.Y., 2010, Densification of nano-SiC by ultra-high pressure effects of time, temperature and pressure, *Fusion Eng. Des.*, 85 (7-9), 964–968.

[22] Lee, Y.I., Kim, Y.W., Mitomo, M., and Kim, D.Y., 2003, Fabrication of dense nanostructured silicon carbide ceramics through two-step sintering, *J. Am. Ceram. Soc.*, 86 (10), 1803–1805.

[23] Noviyanto, A., Han, S.W., Yu, H.W., and Yoon, D.H., 2013, Rare-earth nitrate additives for the sintering of silicon carbide, *J. Eur. Ceram. Soc.*, 33 (15-16), 2915–2923.

[24] Brahmandam, S., and Raj, R., 2007, Novel composites constituted from hafnia and a polymer-derived ceramic as an interface: Phase for severe ultrahigh temperature applications, *J. Am. Ceram. Soc.*, 90 (10), 3171–3176.

[25] Castellan, E., Shah, S.R., and Raj, R., 2010, Compression creep of alumina containing interfacial silicon, carbon, and nitrogen, derived from a polysilazane precursor, *J. Am. Ceram. Soc.*, 93 (4), 954–958.

[26] Noviyanto, A., Yoon, D.H., Han, Y.H., and Nishimura, T., 2016, effect of sintering atmosphere on the grain growth and hardness of SiC/polysilazane ceramic composites, *Adv. Appl. Ceram.*, 115 (5), 272–275.

[27] Zambotti, A., Biesuz, M., Campostrini, R., Carturan, S.M., Speranza, G., Ceccato, R., Parrino, F., and Sorarù, G.D., 2021, Synthesis and thermal evolution of polysilazane-derived SiCN(O) aerogels with variable C content stable at 1600 °C, *Ceram. Int.*, 47 (6), 8035–8043.

[28] Mainzer, B., Lin, C., Jemmali, R., Frieß, M., Riedel, R., and Koch, D., 2019, Characterization and application of a novel low viscosity polysilazane for the manufacture of C- and SiC-fiber reinforced SiCN ceramic matrix composites by PIP process, *J. Eur. Ceram. Soc.*, 39 (2-3), 212–221.

[29] Santoro, U., Novitskaya, E., Karandikar, K., Khalifa, H.E., and Graeve, O.A., 2019, Phase stability of SiC/SiC fiber reinforced composites: The effect of processing on the formation of α and β phases, *Mater. Lett.*, 241, 123–127.

[30] Zhang, X.Y., Li, N., Lan, T., Lu, Y.J., Gan, K., Wu, J.M., Huo, W.L., Xu, J., and Yang, J.L., 2017, In-situ reaction synthesis of porous Si_2N_2O-Si_3N_4 multiphase ceramics with low dielectric constant via silica poly-hollow microspheres, *Ceram. Int.*, 43 (5), 4235–4240.

[31] Li, D., Li, W., Fasel, C., Shen, J., and Riedel, R., 2014, Sinterability of the oxynitride $LaTiO_2N$ with perovskite-type structure, *J. Alloys Compd.*, 586, 567–573.

[32] Gomez, E., Echeberria, J., Iturriza, I., and Castro, F., 2004, Liquid phase sintering of SiC with additions of Y_2O_3, Al_2O_3 and SiO_2, *J. Eur. Ceram. Soc.*, 24 (9), 2895–2903.

[33] Fan, B., Chen, Y., Wang, Y., Liu, G., Zheng, H., Li, H., and Zhang, R., 2021, Preparation of Si_2N_2O wave-transparent and thermal insulation materials with Na_2CO_3 and BN as aids by pressureless sintering, *Ceram. Int.*, 47 (17), 24306–24312.

[34] Jin, H., Jia, D., Yang, Z., and Zhou, Y., 2021,

Mechanical and dielectric properties of direct ink writing Si_2N_2O composites, *J. Eur. Ceram. Soc.*, 41 (4), 2579–2586.

[35] Li, Y., Liu, D., Ge, B., Shi, Z., and Jin, Z., 2018, Fabrication of Si_2N_2O ceramic with silicon kerf waste as raw material, *Ceram. Int.*, 44 (5), 5581–5586.

[36] Lee, S.J., and Baek, S., 2016, Effect of SiO_2 content on the microstructure, mechanical and dielectric properties of Si_3N_4 ceramics, *Ceram. Int.*, 42 (8), 9921–9925.

[37] Bordia, R.K., Kang, S.J.L., and Olevsky, E.A., 2017, Current understanding and future research directions at the onset of the next century of sintering science and technology, *J. Am. Ceram. Soc.*, 100 (6), 2314–2352.

[38] German, R.M., Farooq, S., and Kipphut, C.M., 1988, Kinetics of liquid sintering, *Mater. Sci. Eng., A*, 105-106, 215–224.